Twin Plane Decoration of Silver Nanorods with Palladium by Galvanic Exchange at a Controlled Rate

ARTICLE *in* LANGMUIR · SEPTEMBER 2011

Impact Factor: 4.46 · DOI: 10.1021/la202931m · Source: PubMed

3 AUTHORS, INCLUDING:

Olga Ivanova

Virginia Polytechnic Institute and State Univ…

17 PUBLICATIONS **215** CITATIONS

SEE PROFILE

Langmuir

ARTICLE

pubs.acs.org/Langmuir

Twin Plane Decoration of Silver Nanorods with Palladium by Galvanic Exchange at a Controlled Rate

Grzegorz W. Sławiński, Olga S. Ivanova,[‡] and Francis P. Zamborini*[,†]

[†]Department of Chemistry, University of Louisville, Louisville Kentucky 40292, United States

[‡]Institute of Critical Technologies and Applied Science (ICTAS), Virginia Tech, ICTAS Building, Suite 427, Blacksburg, Virginia 24061, United States

Supporting Information

ABSTRACT: Here we describe the galvanic exchange of surface-grown Ag nanorods (NRs) and nanowires (NWs) with $PdCl_4^{2-}$ as a function of the $PdCl_4^{2-}$ concentration. The morphology of the resulting AgPd alloy nanostructures depends on the galvanic exchange rate, which increases with increasing $PdCl_4^{2-}$ concentration over a specific concentration range. When the concentration of $PdCl_4^{2-}$ exceeds 7.5×10^{-5} M (or ratio of moles of $PdCl_4^{2-}$ in solution to moles of Ag on the surface > 542), rapid galvanic exchange results in Pd deposition over the entire Ag nanostructure in the early stages of exchange. When the concentration of $PdCl_4^{2-}$ is in the range of 1.0×10^{-5} to 5.0×10^{-5} M (moles of $PdCl_4^{2-}$ in solution to moles of Ag on the surface = 13−54), Pd deposition occurs preferentially at high energy twin plane defects in the form of well-spaced nanoparticles during the early stages of exchange. In later stages, the Pd deposits grow and coalescence into a rough shell, and etching of the Ag leads to a presumably hollow nanostructure. Composition analysis by linear sweep voltammetry as a function of time shows that the galvanic exchange rate is much slower than the diffusion-limited rate and, when correlated with UV−vis spectroscopy, shows that less than 10% Pd in the nanostructure completely dampens the Ag-localized surface plasmon band.

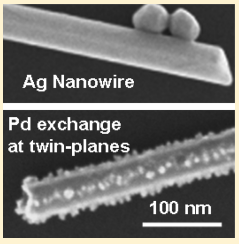

INTRODUCTION

Metallic nanostructures have attracted a tremendous amount of attention in recent years because of their interesting size-, shape-, and composition-dependent properties[1−5] and potential use in photonics,[6] catalysis,[7,8] nanoelectronics,[9] chemical sensing,[10] and biomedical applications.[11] One-dimensional (1D) metal nanostructures are of particular interest to our group because of their possible use in sensing and catalysis applications. Several methods exist for the chemical synthesis of 1D nanometals, including UV irradiation, seed-mediated growth, and the polyol process.[12−32]

Although monometallic nanostructures have several useful properties and applications, there are cases where bimetallic or multimetal nanostructures are desirable. There are several methods for synthesizing bi- or multimetal nanostructures, including the seeded growth of one metal onto another,[33] the coreduction of two metal salts in the presence of a stabilizer,[34] or the galvanic exchange[35−37] method. In galvanic exchange, a metal in the reduced form becomes replaced by a metal in the oxidized form by a simple oxidation−reduction reaction. The requirement is that the metal initially in the reduced form has a more negative reduction potential than the metal initially in the oxidized form. Because the metal in the reduced form requires more energy to be reduced than the metal in the oxidized form, this will lead to spontaneous replacement via oxidation of the reduced metal and reduction of the oxidized metal.

Several processes occur during galvanic exchange reactions. The solid metal structure becomes oxidized (dissolved), and metal ions from solution become reduced (deposited) onto the original template structure. At an intermediate point before the reaction is complete, the metal undergoing reduction may alloy with the second metal. As the second metal dissolves, this usually involves a dealloying process. Reactions 1−3 show the possible reactions that occur, where M1 represents a metal initially in the reduced form and M2 represents a metal (ion or complex) in the oxidized form. Reaction 1 is the combined full reaction. Reactions 2 and 3 represent alloying and dealloying processes.[38]

$$M1_{red} + M2_{ox} \rightarrow M1_{ox} + M2_{red} \text{ (complete reaction)} \quad (1)$$

$$2M1_{red} + M2_{ox} \rightarrow M1_{ox} + M1M2_{alloy} \text{ (alloying)} \quad (2)$$

$$M1M2_{alloy} + M2_{ox} \rightarrow M1_{ox} + 2M2_{red} \text{ (dealloying)} \quad (3)$$

The galvanic exchange reaction is a well-known oxidation−reduction reaction commonly shown in most general chemistry textbooks but has recently attracted attention as a useful method for synthesizing interesting nanoscale metallic structures.[35−37,39] It is a simple spontaneous reaction that can be controlled and stopped at a desired time or the metals can be combined in a certain ratio to obtain the desired composition of the final metallic nanostructure. In addition, the morphology of the final exchanged nanostructure is often unique and not easily synthesized by direct metal ion reduction methods. For example, Xia and co-workers titrated Ag nanowires with $HAuCl_4$ and Pd$(NO_3)_2$ solutions to obtain unique hollow nanotubes with two or three coaxial walls made of AuAg or PdAg alloys.[37,40,41] The reaction of cubic Ag nanostructures with $HAuCl_4$ led to the

Received: July 28, 2011
Revised: September 13, 2011
Published: September 14, 2011

formation of cubic Au nanocages.[39] In a similar fashion, Ag or AuAg alloys treated with $AuCl_4^-$, $PtCl_4^{2-}$, or Pd(II) salts led to the formation of nanorattles, nanoshells, nanocubes, nanocages, nanoboxes, and nanoframes.[39,42−45] The galvanic exchange of Pd nanowires with Au salt led to the formation of tadpolelike structures consisting of a Au head and Pd tail.[46] Others used galvanic replacement to form nanoporous Cu−Ni films,[47] hollow metallic or bimetallic urchinlike Pt or Pd nanostructures,[48,49] Pt nanofibers and nanotubes,[48] Pt-coated nanoporous Au nanorods,[50] Pd−Au nanostructures,[51] Ag−Au bimetals,[43] hollow Pt and Au nanoshells,[52,53] nanotaper ZnO[54] tubes, and superhydrophobic Ag-coated films on a copper surface.[55,56] Examples of Ag exchanged specifically with Pd(II) salts include PdAg in carbon spheres,[57] nanoneedle-covered PdAg nanotubes,[58] and dendritic PdAg alloys.[59,60] Our group previously synthesized Ag NRs/NWs and formed hollow Pd nanotubes and Au/Pd core/shell nanostructures using the galvanic replacement reaction directly on surfaces.[61]

By using galvanic exchange, many of the structures synthesized exhibit unique and tunable properties that are not accessible by other synthesis methods. This can lead to new applications. For example, the optical properties of AuAg nanostructures could be tuned by controlling the galvanic exchange of Ag nanoboxes with $HAuCl_4$.[39] Xia and co-workers tuned the optical properties of galvanically exchanged metal nanostructures in the near-IR region where human tissue has the highest transmission for applications in tumor treatment.[43] Other nanostructures obtained through galvanic exchange were useful for surface-enhanced Raman spectroscopy (SERS),[39,43,45,59,62,63] catalysis,[58,60,64−68] and hydrogen storage/sensing.[42,45,46]

Although many groups use the galvanic exchange method to synthesize novel metallic structures with interesting properties, there are few detailed mechanistic studies of the process. Xia and co-workers recently studied the mechanism of the galvanic exchange reaction between Ag and various metal salts (usually $HAuCl_4$) in aqueous or organic media on nanoparticles, nanoplates, NRs, nanoboxes, and twinned nanoparticles.[36−38,69,70] In general, with Au as the example, the replacement occurs through the steps of (1) Ag oxidation, (2) Au deposition, (3) AuAg alloy formation, and (4) dealloying of Ag. In the first step, pitting (oxidation) of the Ag nanostructure occurs, followed by the epitaxial growth of Au onto the remaining Ag. The Ag and Au then alloy. If the reaction is stopped at this stage, then the nanostructure is usually a closed AuAg alloy structure similar to the original Ag template, but with a hollow interior. Continuing the reaction leads to the dealloying of Ag from AuAg, which may lead to caged structures or broken/collapsed nanostructures.

The details of the final nanostructure depend on many factors, including the initial size and shape of the Ag nanostructure, temperature, and strength of the capping agents used. For example, a Ag cube with sharp edges has mainly (100) surfaces that preferentially etch during exchange, and a truncated Ag cube has (111) facets exposed at the corners.[36,71] The (111) regions preferentially etch in the presence of the capping agent, leading to a hollow structure with pores at the corners or a different type of caged structure after further dealloying.[36,71] Smaller Ag nanostructures behave differently compared to larger structures because of the larger number of defects and greater propensity to alloy and because twinned structures tend to alloy better.[69] In the case of Ag plates, if they are not thick enough, then a full shell of Au cannot form and an Au ring results.[37] If the plate is thick enough, then a full hollow structure forms.[37] Xia and co-workers also studied the effect of temperature, showing that it played a key role because of the increased solubility of AgCl and enhanced diffusion of metal atoms at higher temperature.[70] The capping agent can effect the exchange by binding to different metal crystal faces with different strengths and also effecting the solubility of AgCl or other reaction products.[69]

Although the work of Xia and others has led to a better understanding of the galvanic exchange process on the nanoscale, especially for the exchange of Ag with $AuCl_4^-$, there are still several details that are not fully understood. There is a need for detailed studies on other metal pairs and on the effect of other variables, such as the reaction rate, solvent, presence or lack of stabilizers (surfactants, polymers), and the presence or lack of other additives (such as ions)[72] in solution, on the galvanic exchange process. The goal of our research is to understand better the effect of these variables on the morphology of galvanically exchanged metal nanostructures and to use the knowledge gained to create unique structures with useful properties for sensing and catalysis applications.

Here we describe the effect of the rate of galvanic exchange on the morphology of the resulting nanostructure for Ag NRs/NWs exchanged with $PdCl_4^{2-}$ directly on surfaces. There are several differences between this work and previous studies. First, we describe the exchange of Ag nanostructures that are attached to a surface as opposed to being freely suspended in a solution. Importantly, this allows us to study the galvanic exchange reaction under a much wider range of conditions (different solvents, stabilizers, additives, concentrations, and temperatures) because we do not need to suspend the nanostructures in solution, which may allow us to follow the galvanic exchange process on an individual nanostructure in the future. Second, we describe the effect of the galvanic exchange rate on the morphology of the resulting nanostructure, an important variable that has not been studied in detail previously. Third, we describe a new exchange mechanism for Ag with $PdCl_4^{2-}$ not previously reported because most of the work focused on Ag exchanged with $AuCl_4^{2-}$. Fourth, we describe the exchange under surfactant-free conditions, which is possible only because the exchange occurs on a surface. In the reports cited here, mainly the exchange of nanostructures in solution and in the presence of a surfactant or polymer stabilizer were studied; these can have a large effect on the exchange process because of the different binding strengths of the stabilizer to the various metal crystal faces and potential precipitation with the metal ions involved. Zhao and co-workers recently described the exchange of Zn films with Ag^+ in the presence of various polymers, surfactants, and salt additives, showing large differences in Ag morphology based on these effects.[73] In our previous study of Ag nanowire synthesis[61,74] and exchange,[61] the reaction occurred at a relatively large $PdCl_4^{2-}$ concentration at a fast rate. This work is different because we control the rate by varying the $PdCl_4^{2-}$ concentration and show that the morphology of the galvanically exchanged PdAg nanostructures strongly depends on the reaction rate. Lastly, we describe the use of anodic stripping voltammetry to approximate the amount of Ag and Pd in the nanostructures at various exchange times, which allows us to understand better the reaction kinetics and correlate the optical properties with the composition of the metallic nanostructures. This work represents new methodology and information that is important for better understanding and controlling the galvanic exchange process in order to fine tune the metal nanostructure composition and morphology for a wide range of applications.

EXPERIMENTAL SECTION

Chemicals and Materials. Silver nitrate ($AgNO_3$, 99+%), sodium borohydride ($NaBH_4$, 98%), potassium tetrachloropalladate(II) (K_2PdCl_4, 98%), and L-ascorbic acid (99.9%) were purchased from Sigma-Aldrich. Hydrogen tetrachloroaurate trihydrate ($HAuCl_4 \cdot 3H_2O$) was synthesized according to a literature procedure.[75] Citric acid trisodium salt was purchased from Bio-Rad Laboratories. Sodium phosphate dibasic and sodium phosphate tribasic were purchased from Fisher Scientific Company. Potassium bromide (min 99.0%), perchloric acid (60%), hydrogen peroxide (H_2O_2 30% solution), and 2-propanol (HPLC grade, 99.99%) were purchased from EMD. Sulfuric acid was purchased from BDH Aristar (distributed by VWR). Cetyltrimethylammonium bromide (CTAB) was purchased from Fluka (assay ≥99.0%). NANOpure ultrapure water (Barnstead Nanopure deionization system, resistivity of 18MΩ·cm) was used for all aqueous solutions. Indium tin oxide (ITO)-coated glass (Glass/ITO, Rs = 8−12 Ω) substrates were purchased from Delta Technologies Limited (Stillwater, MN).

Synthesis of Ag Nanostructures Directly on Surfaces. We synthesized Ag nanostructures directly on surfaces by a seed-mediated growth method as described previously.[61,74] First, glass, Si/SiO_x, or glass/indium tin oxide (glass/ITO) substrates were cleaned and functionalized with mercaptopropyltrimethoxysilane (MPTMS). The MPTMS-functionalized substrates were then placed in an aqueous solution of 3−5 nm diameter Au seed nanoparticles (Au NPs)[76,77] for 20 min. Finally, substrate/MPTMS/Au NP samples were placed in an Ag growth solution containing 10 mL of pH 10.6 phosphate-buffered 0.08 M CTAB, 250 μL of 0.01 M $AgNO_3$, and 500 μL of 0.1 M ascorbic acid for 30 min in a 28 °C temperature bath. This procedure leads to Ag nanostructures on the surface with a density of 26 ± 14 μm^{-2} and an ∼3% yield of 1D Ag nanorods (NRs) and nanowires (NWs) on the surface with a diameter of 34 ± 14 nm and lengths ranging from 200 nm to 10 μm.[61] Because most of the structures have an aspect ratio (AR) of greater than 20, we will refer to all 1D nanostructures as NWs in the text, even though some may technically be NRs (AR < 20).

Galvanic Exchange between Ag NRs/NWs and $PdCl_4^{2-}$. The surface-attached (glass or Si/SiO_x)/MPTMS/Ag NWs were placed into aqueous 0.01, 0.001, 0.0001, 0.000075, 0.000050, 0.000025, or 0.000010 M K_2PdCl_4 solutions for times ranging from 0 to 3600 s. Galvanic exchange occurred extremely fast for concentrations of 0.01 and 0.001 M; therefore, the results focus on the range from 1.0×10^{-4} to 1×10^{-5} M. Ag-coated glass, Si/SiO_x, and glass/ITO samples were placed in the appropriate aqueous $PdCl_4^{2-}$ solutions for a desired period of time, removed, rinsed with nanopure H_2O, and dried under a stream of nitrogen prior to UV−vis, scanning electron microscopy (SEM), and anodic stripping voltammetry analysis, respectively.

Electrochemical Characterization by Linear Sweep Voltammetry. We developed a compositional analysis by linear sweep anodic stripping voltammetry in order to obtain the approximate metal composition of the galvanically exchanged nanostructures. We used a three-electrode setup where glass/ITO/MPTMS/Ag nanostructures (before and after galvanic exchange with $PdCl_4^{2-}$) served as the working electrode, Ag/AgCl (3 M KCl) served as a reference, and a Pt wire served as a counter electrode. We ran the first linear sweep voltammogram (LSV) in 0.5 M H_2SO_4 from 0.0 to 0.6 V at 10 mV/s in order to obtain an Ag oxidation (or stripping) peak. Next, the sample was gently rinsed in nanopure H_2O, and a second LSV scan was obtained in 0.01 M KBr plus 0.1 M $HClO_4$ from 0.0 to 0.8 V at 10 mV/s in order to monitor the Pd stripping peak. LSVs were analyzed, and the amounts of Ag and Pd in the nanostructures were determined by integrating the areas under the oxidation peaks.

Instrumentation. Scanning electron microscopy images were obtained at different magnifications using a Carl Zeiss SMT AG Supra 35VP field emission scanning electron microscope (FESEM) operating at an accelerating voltage of 5.00 to 20.00 kV and using an in-lens ion annular secondary electron detector. UV−vis spectra were obtained using a Varian Cary 50 Bio UV−visible spectrophotometer. A CH Instruments (Austin, TX) 630C electrochemical analyzer/workstation was used for the electrochemical stripping analysis of Ag and galvanically exchanged AgPd alloy nanostructures.

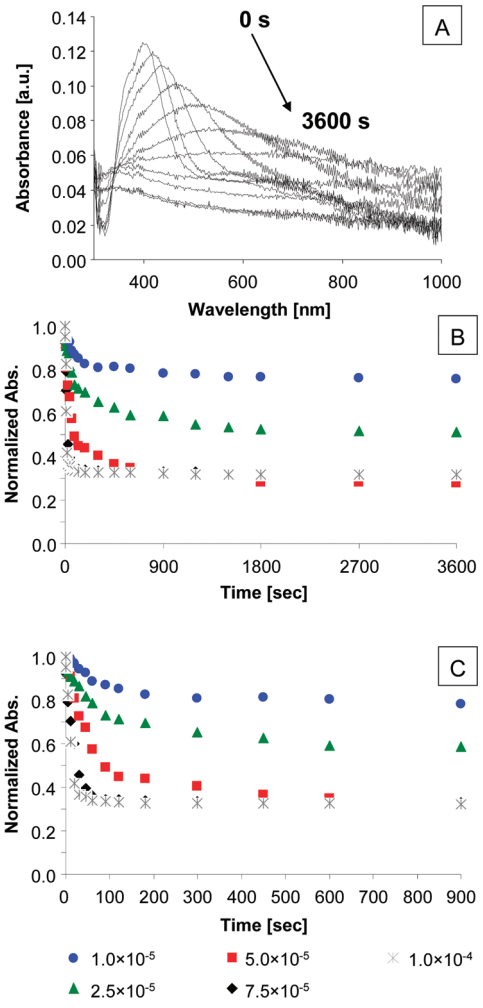

Figure 1. (A) UV−vis spectra of Ag nanostructures on glass exchanged with 5.0×10^{-5} M $PdCl_4^{2-}$ for 0 to 3600 s. (B) Change in the normalized absorbance of the Ag surface plasmon band with time during exchange with 1.0×10^{-5}, 2.5×10^{-5}, 5.0×10^{-5}, 7.5×10^{-5}, and 1.0×10^{-4} M $PdCl_4^{2-}$. (C) Enlargement of the plot in B from 1 to 900 s.

RESULTS AND DISCUSSION

Most previous galvanic exchange studies occurred in solutions containing a stabilizer (polymer or surfactant) with the final metal composition controlled by the ratio of the reduced metal and the oxidized metal in solution, where the reaction went to completion. Although the morphology of the final product can be obtained as a function of the final composition, the effect of the exchange rate in stabilizer-free solutions can not be determined. Here we describe the results for the galvanic exchange of Ag with $PdCl_4^{2-}$. The optical and electrochemical measurements reflect the entire surface, which contains 97% spherical nanoparticles and 3% Ag NWs, and the SEM images focus on the morphology of the Ag NWs because of our interest in 1D nanostructures. Because we synthesized the Ag nanostructures directly onto

dx.doi.org/10.1021/la202931m |*Langmuir* 2011, 27, 13293–13301

surfaces, we were able to study the exchange in stabilizer-free aqueous solutions and control the rate of exchange by varying the $PdCl_4^{2-}$ concentration, which alters the flux of $PdCl_4^{2-}$ to the surface.

Figure 1A shows the UV−vis spectra of a sample of Ag nanostructures grown on glass before and at various times during galvanic exchange with an aqueous 5.0×10^{-5} M $PdCl_4^{2-}$ solution from 0 to 3600 s. (See Figure S1 in the SI for all concentrations.) The reaction between Ag^0 and $PdCl_4^{2-}$ occurs spontaneously as follows:

$$2Ag^0(s) + PdCl_4^{2-}(aq) \rightarrow Pd^0(s) + 2AgCl(s \text{ or } aq) + 2Cl^-(aq) \quad (4)$$

At 0 s of exchange, the pure Ag nanostructures exhibit a prominent, well-known localized surface plasmon (LSPR) band at about 420 nm. As the exchange with $PdCl_4^{2-}$ proceeds, the Ag LSPR band decreases in intensity and red shifts as shown previously.[61] This is consistent with Pd deposition and Ag oxidation as the Ag nanostructures transform into PdAg alloy nanostructures and eventually Pd if the exchange goes to completion.

Figure 1B shows the normalized peak absorbance of the LSPR band as a function of exchange time for exchange with 5.0×10^{-5} M $PdCl_4^{2-}$ and four other concentrations of $PdCl_4^{2-}$ ranging from 1.0×10^{-5} to 1.0×10^{-4} M as shown. (See Figure S2 in the SI for plots with standard deviations.) The absorbance values were measured at the LSPR peak maxima. At later stages of exchange, when the peaks became broad and flat, the absorbance was extrapolated to the line where the peak maxima would have been as an estimate. The plots show an increasing rate of exchange with increasing $PdCl_4^{2-}$ concentration. Frame C shows an enlarged image of the plot in frame B from 0 to 900 s. To estimate the rate of exchange, we calculated the initial slope of the curve over the first 30 s. The slopes of the plots for 1.0×10^{-4}, 7.5×10^{-5}, 5.0×10^{-5}, 2.5×10^{-5}, and 1.0×10^{-5} M $PdCl_4^{2-}$ concentrations were 0.0211, 0.0181, 0.0092, 0.0045, and 0.0019, respectively.

Figure 1B also shows that the Ag nanostructures exchanged with the two lowest $PdCl_4^{2-}$ concentrations do not reach the same level of completion after 3600 s when compared to those exchanged with 5.0×10^{-5} M $PdCl_4^{2-}$ or higher, which all have the same final normalized absorbance value at about 0.3. On the basis of the calculated 3.7×10^{-8} mol Ag on the surface obtained from linear sweep voltammetry (average of 16 samples), the ratio of the total number of moles of $PdCl_4^{2-}$ in solution to the total number of moles of Ag on the surface ranges from 13 to 542 for the range of 1.0×10^{-5} to 1.0×10^{-4} M $PdCl_4^{2-}$. There is clearly enough total moles of $PdCl_4^{2-}$ in the entire solution to exchange with all of the Ag on the surface, especially considering that one Pd(II) will exchange with two Ag^0 atoms. Also, thermodynamics indicates that the driving force is large enough to replace Ag fully with Pd.

Even though there is enough $PdCl_4^{2-}$ in the ∼20 mL volume solution to replace all of the Ag, not all of the $PdCl_4^{2-}$ will reach the surface within the 3600 s reaction time. The amount of $PdCl_4^{2-}$ that reaches the surface with time, assuming linear diffusion, is given by

$$\text{mol} = \frac{2ACD^{1/2}t^{1/2}}{\pi^{1/2}} \quad (5)$$

where A is area of the substrate, C is the concentration, D is the diffusion coefficient (1.0×10^{-5} cm^2/s),[78] and t is time. After 3600 s, 9.6×10^{-9} to 9.6×10^{-8} total mole of $PdCl_4^{2-}$ reaches the substrate surface for the 1.0×10^{-5} to 1.0×10^{-4} M $PdCl_4^{2-}$ concentrations, respectively. After 3600 s with a 1.0×10^{-5} M $PdCl_4^{2-}$ concentration, the amount of $PdCl_4^{2-}$ reaching the surface could oxidize a maximum of 1.9×10^{-8} mole of Ag (2(9.6×10^{-9} mole of Pd(II))), assuming every $PdCl_4^{2-}$ anion reacted. This is less than the 3.7×10^{-8} mole of Ag on the surface, making it impossible for the reaction to reach completion in this time frame. Table 1 shows the concentration of $PdCl_4^{2-}$, the moles of $PdCl_4^{2-}$ that reach the surface in 3600 s, the maximum amount of Ag that could be oxidized, and the percent of Ag that would be left in the nanostructure if fully reacted. Concentrations of 2.5×10^{-5} M or higher have enough $PdCl_4^{2-}$ to exchange Ag fully after 3600 s. Table 1 also shows the average concentrations of Ag^+ and Cl^- in the diffusion layer (∼3.4 mL based on $2(Dt)^{1/2}$) and the product $[Ag^+][Cl^-]$. The product is larger than the K_{sp} for AgCl(s) (1.8×10^{-10} M^2) for $PdCl_4^{2-}$ concentrations of 2.5×10^{-5} M or more. This indicates that AgCl(s) likely forms on the nanostructures for the galvanic exchange under those conditions at room temperature. Over time, the AgCl should eventually dissolve once mixed throughout the entire 20 mL volume.

To determine how the rate of galvanic exchange affects the morphology of the exchanged structure, we conducted exchange reactions at three different concentrations and stopped them at the same level of exchange as judged by the normalized UV−vis absorbance value. Figure 2 shows SEM images of Ag NWs galvanically exchanged according to eq 1 with 2.5×10^{-5}, 5.0×10^{-5}, and 7.5×10^{-5} M $PdCl_4^{2-}$ until the normalized absorbance reached ∼0.6. Assuming that the absorbance is closely related to the composition, these AgPd NWs should have similar compositions that are reached at different rates. In fact, it took 600, 60, and 20 s, respectively, with increasing $PdCl_4^{2-}$ concentration, to reach the normalized value of 0.6. This again shows that the higher concentration $PdCl_4^{2-}$ solutions led to a faster galvanic exchange reaction rate. On the basis of the electrochemical composition analysis shown later, these samples contain ∼90% Ag, indicating that this is very early in the exchange process. The main conclusion from the images is that the morphology of the nanostructures depends on the rate of galvanic exchange for a constant final composition. For the lowest rate of exchange (2.5×10^{-5} M $PdCl_4^{2-}$), the twin-plane defects of the Ag NWs are decorated with a high density of fairly small Pd nanoparticle deposits. At 5.0×10^{-5} M, the twin planes are also decorated with Pd nanoparticles, but the density is lower and the particles are larger. At the fastest rate (7.5×10^{-5} M), Pd deposits grow in the form of nanoparticles more or less evenly all over the Ag NW. From these images, it is not clear where the Ag oxidation occurs. This is the first demonstration to our knowledge of different morphologies of 1D-exchanged metal as a function of the exchange rate in the absence of surfactants or polymer stabilizers.

We found the twin-plane-decorated Ag NWs to be fascinating, unique structures and decided to study the exchange process on these NWs in greater detail. Figure 3 shows SEM images of different samples of Ag NWs at different stages of exchange with 5.0×10^{-5} M $PdCl_4^{2-}$, where twin-plane decoration occurs in the early stages. Frame A of Figure 3 shows a representative structure of an Ag NW grown directly on Si/SiO_x before the galvanic exchange. The NW has smooth edges and a uniform diameter along the entire length. The NW structure is known to be multiply twinned with 5-fold symmetry and a pentagonal cross section.[79] One of the twin planes is faint but observable along the

Table 1. Calculated Concentrations of Reactants and Products That Would Be Formed at the Electrode Surface after 3600 s of Reaction Time for Various Concentrations of $PdCl_4^{2-}$ if the Reaction Kinetics Were Diffusion-Controlled

$[PdCl_4^{2-}]_{initial}$ (M)	moles of $PdCl_4^{2-}$ required to reach the surface in 3600 s	maximum mols of Ag^+ formed in 3600 s	maximum mols Cl^- formed in 3600 s	$[Ag^+]_{av}$ in 3.4 mL volume (M)	$[Cl^-]_{av}$ in 3.4 mL volume (M)	$[Ag^+][Cl^-]$ (M^2)	% Ag left after 3600 s
1.0×10^{-5}	9.6×10^{-9}	1.9×10^{-8}	3.8×10^{-8}	5.6×10^{-6}	1.1×10^{-5}	6.2×10^{-11}	49
2.5×10^{-5}	2.4×10^{-8}	3.7×10^{-8}	9.6×10^{-8}	1.1×10^{-5}	2.8×10^{-5}	3.1×10^{-10}	0
5.0×10^{-5}	4.8×10^{-8}	3.7×10^{-8}	1.9×10^{-7}	1.1×10^{-5}	5.6×10^{-5}	6.2×10^{-10}	0
7.5×10^{-5}	7.2×10^{-8}	3.7×10^{-8}	2.9×10^{-7}	1.1×10^{-5}	8.5×10^{-5}	9.4×10^{-10}	0
1.0×10^{-4}	9.6×10^{-8}	3.7×10^{-8}	3.8×10^{-7}	1.1×10^{-5}	1.1×10^{-4}	1.2×10^{-9}	0

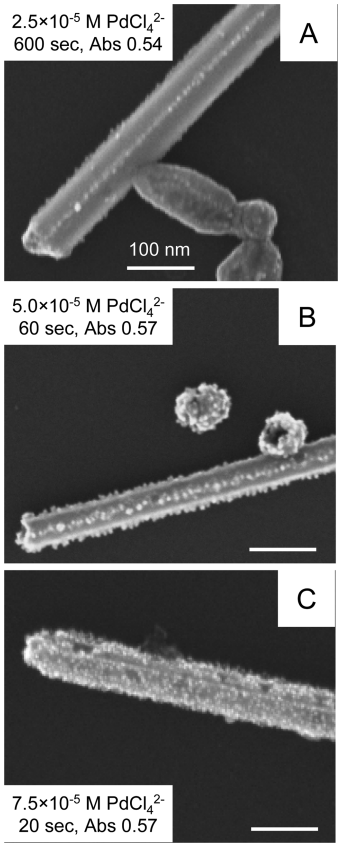

Figure 2. SEM images of galvanically exchanged nanostructures with different $PdCl_4^{2-}$ concentrations with matching absorbance values (0.6).

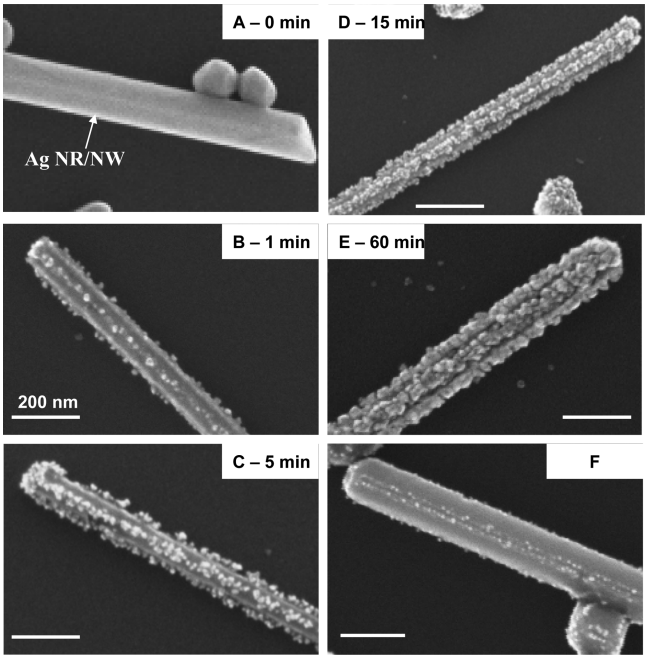

Figure 3. SEM images of progressing the galvanic exchange with time for 5.0×10^{-5} M $PdCl_4^{2-}$ in H_2O. (A–E) Ag NW during the galvanic exchange at 0, 1, 5, 15, and 60 min, respectively. (F) Double defect at the twin plane along the entire length of the Ag NW.

center of the NW. Frames B–E show different Ag NWs following galvanic exchange with a 5.0×10^{-5} M $PdCl_4^{2-}$ solution for 1, 5, 15, and 60 min as indicated. Frame B shows that the reduction of Pd again occurs favorably at the Ag NW twin-plane defect and deposited as well separated nanoparticles. With an increasing exchange time, the Pd particles grow in size while Ag dissolves, and after approximately 15 min (Frame D), the Pd NPs coalesce with neighboring particles and form a continuous structure along the twin planes of the original Ag NW. After 60 min of reaction, the nanostructure is significantly roughened, but it is still clear that the exchange emanated from the twin planes.

The original Ag NWs are multiply twinned structures with 5-fold symmetry where the cross section is a pentagonal shape, the ends of the NRs/NWs contain five (111) facets, and the long axis contains (100) or (110) facets.[17,23,79] These 1D structures grow from multiply twinned decahedral particles.[42] The theoretical angle between two (111) planes is 70.52°. Because $5 \times 70.52° = 352.60°$, there is a misfit angle of 7.4° to complete 360° as described by Chen and Gao.[15,79] We believe that this is the reason for the double parallel lines of Pd that we often observe at the twin-plane defects such as those shown in Figure 3F.

Scheme 1 shows a proposed mechanism for the galvanic exchange reaction. The twin plane of the Ag NW is a defect site of the crystal lattice. It is well known that defect sites are more reactive than defect-free crystallographic terraces.[80] Step A in Scheme 1 shows the pentagonal cross section of the Ag NW structure. In most cases, on the basis of SEM images, the Ag NWs grow on the surface showing only three twin planes and the other two are bound to the surface as shown. Step B shows the deposition of Pd on the defect sites (twin planes) of an Ag NW. Steps C–F show more deposition of Pd on the Ag while the Ag is removed as Ag^+, presumably from the terraces and interior of the Ag NW. The continuation of this process leads to the structures shown in Figure 3E. On the basis of previous work, we believe that the final structures are hollow.[28] Figure S3 shows

Scheme 1. Model of the Galvanic Exchange Reaction with the Preferential Decoration of Twin-Plane Defects with Time

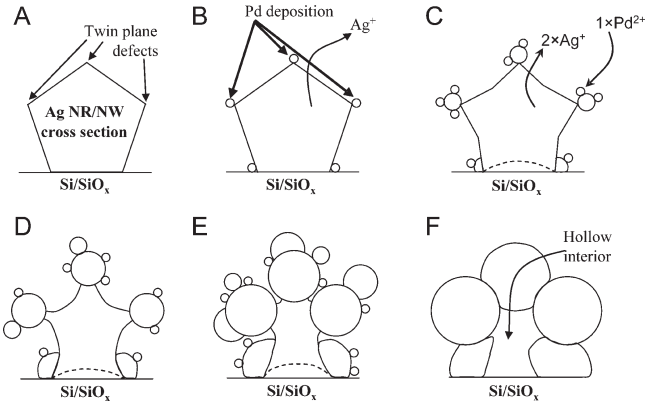

examples of apparently hollow exchanged PdAg structures, but the SEM images are not conclusive.

The structures shown in Figure 3 are markedly different from the smooth Pd or PdAg hollow nanotubes previously synthesized by others by the galvanic exchange of Ag NRs with Pd(II) complexes.[37,40,41,45] The images in Figures 2 and 3 show nanostructures with the deposition of metal along the twin-plane defects. If one considers only the deposition step, then it is reasonable that Pd would deposit onto the high-energy twin-plane defect sites. It is possible that the previous studies on PdAg simply did not observe the exchange in this early stage. Our structures may be rougher in the end because of the precipitation of AgCl on the surface.[70] In previous studies of Ag nanostructures exchanged with $HAuCl_4$, the process led to the formation of pits on the surface, usually at facets, in early stages.[36−38,69,70] Our mechanism could be different because of the different metal, the lack of stabilizer in our case, the lower temperature, and the fact that the reaction occurred on surface-attached nanostructures. We note that Bi and co-workers observed the twin-plane decoration of Ag NWs with Pt during galvanic exchange in surfactant-containing solutions, where their goal was to synthesize a high yield of platinum nanowires.[48]

An important question that arose in this work was how the normalized intensity of the LSPR band correlates with the Ag and Pd composition in the nanostructures. We used linear sweep voltammetry to estimate the Ag and Pd composition on glass/ITO electrodes very roughly during the galvanic exchange process in order to correlate the composition to the normalized absorbance. First, we acquired the Ag oxidation peak by obtaining a linear sweep voltammogram (LSV) of glass/ITO/AgPd electrodes in 0.5 M H_2SO_4 from 0 to 0.6 V. Next, we obtained LSVs of the same electrode from 0 to 0.8 V in 10 mM KBr + 0.1 M $HClO_4$ solution to acquire the Pd oxidation peak. The oxidation reactions for Ag and Pd are as follows:

$$Ag(s) \rightarrow Ag^{+}(aq) + 1e^{-} \quad (6)$$

$$Pd(s) + 4Br^{-}(aq) \rightarrow PdBr_4^{2-}(aq) + 2e^{-} \quad (7)$$

Figure 4A,B shows LSVs of galvanically exchanged Ag nanostructures after different exchange times with 5.0×10^{-5} M $PdCl_4^{2-}$, which correlates with the SEM images in Figure 3 and the UV−vis data in Figure 1A. Figure 4A shows that the amount

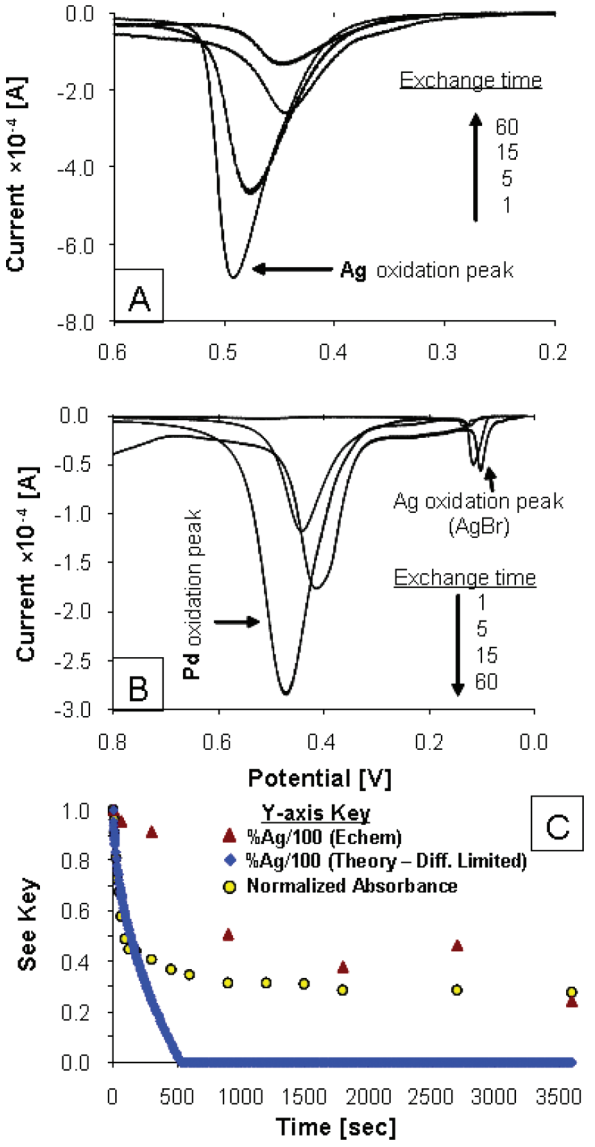

Figure 4. (A, B) LSVs of ITO/MPTMS/Au seed/AgNW after exchange with 5.0×10^{-5} M $PdCl_4^{2-}$. (A) Ag oxidation in 0.5 M H_2SO_4. (B) Pd oxidation in 0.01 M KBr in 0.1 M $HClO_4$. (C) Comparison among experimental UV−vis (yellow circles), experimental electrochemical (red triangles), and theoretical (calculated) (blue diamonds) amounts of Ag present on the sample under the 5.0×10^{-5} M condition.

of Ag in the sample decreases with time during the exchange, as determined from the decreasing area under the Ag oxidation peak at 450−500 mV with increasing exchange time. This is expected because Pd replaces Ag during the exchange. After 60 min of exchange, the Ag peak is still visible, showing that not all of the Ag became oxidized during the reaction. Figure 4B shows that the Pd oxidation peak near 400−480 mV increases as a function of the exchange time, consistent with Pd deposition on the surface during the replacement of Ag. The peak at ~0.1 V is due to the oxidation of Ag (to form AgBr) that remained on the surface after the first scan in H_2SO_4. The amount of leftover Ag determined from the peak at 0.1 V during the scan in KBr in Figure 4B is less than 10% of the Ag oxidation in H_2SO_4 (Figure 4A), representing a small error in the measured amount of Ag. We used the LSV data to calculate the ratio of the moles of

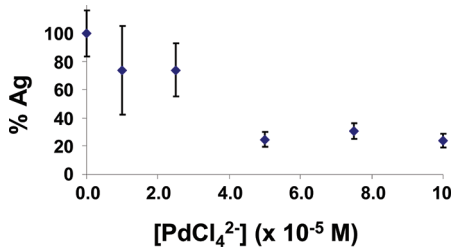

Figure 5. % Ag vs $PdCl_4^{2-}$ concentration used for the galvanic exchange after 3600 s.

Ag and Pd present in the sample to estimate very roughly the composition of the nanostructures. The following equation gives the moles of metal from the measured coulombs of charge (Q) under the LSV peaks in Figure 4A,B, the Faraday constants (F), and the number of electrons involved in the oxidation (n):

$$\text{mol} = \frac{Q}{nF} \tag{8}$$

Figure 4C shows a comparison of the experimental galvanic exchange data obtained by normalized absorbance (yellow circles) with the composition determined by LSV (red triangles) and also shows a theoretical plot of the %Ag as a function of time based on the assumption that all of the $PdCl_4^{2-}$ molecules reacted with Ag on the surface at a diffusion-controlled rate (blue diamonds) as determined by eq 5. If every molecule of $PdCl_4^{2-}$ reaching the surface reacted with Ag, then the %Ag would decrease as shown by the blue diamonds in Figure 4C, which is the fastest possible rate of reaction (Figure S4 shows similar plots with other $PdCl_4^{2-}$ concentrations and Figure S5 shows LSV data of both Ag and Pd with the exchange time).

There are three important points to note in the plots of Figure 4C. First, the actual composition of Ag does not track well with the normalized visible absorbance. With only about 10% of Pd in the nanostructure, the LSPR band of the Ag drops close to its lowest value. An additional increase in Pd and the loss of Ag do not alter the normalized absorbance appreciably after that. Therefore, the UV−vis data do not reflect the composition and kinetics of the entire exchange process accurately. It most likely reflects the kinetics and composition of Pd and Ag only at the surfaces of the nanostructures because the LSPR band is a surface phenomenon. Second, the theoretical plot of %Ag versus the exchange time, based on diffusion-limited reactivity, does not match well the actual composition of Ag with time determined by LSV. The actual rate is much slower than that expected for a diffusion-controlled process. Theoretically, all of the Ag should be oxidized after about 520 s, whereas in actuality, ∼70% of the Ag remained on the surface after 500s and 30% remained after 3600 s. Related to this, the third point is that the reaction does not reach completion. This could not have been determined by SEM or UV−vis alone. Some Ag remained stable for very long times. It may be trapped in the interior of the structure and not accessible to react with $PdCl_4^{2-}$, or it may have alloyed with Pd to form more stable AgPd. This would shift the thermodynamics of the Ag oxidation.

Because we observed that not all of the Ag oxidized following 3600 s of exchange with 5.0×10^{-5} M $PdCl_4^{2-}$, we determined the amount of Ag in the nanostructures exchanged after 3600 s for the other $PdCl_4^{2-}$ concentrations. Figure 5 shows a plot of % Ag as a function of the concentration of $PdCl_4^{2-}$ used in the exchange after 3600 s. Interestingly, the three highest concentrations show the same amount of Ag in the final structure (20−30%). These three samples also had similar final normalized absorbance values (Figure 1). The final AgPd seems to reach a stable value, independent of the $PdCl_4^{2-}$ concentration or rate of exchange for these concentrations. This value is similar to the final 25% Ag observed by Sun and Xia during replacement with high concentrations of $HAuCl_4$.[41] The %Ag is around 70−80% for exchange with the two lower $PdCl_4^{2-}$ concentrations. The larger value of Ag is consistent with the larger normalized absorbance in the UV−vis spectra (Figure 1), but the LSV is more quantitative.

We emphasize that the LSV provides only an estimate of the Ag and Pd composition. If some metal is not accessible for oxidation during LSV, then this would lead to error, where the calculated number of moles would be smaller than the actual value. If the error is similar for Pd and Ag, then the mole ratio would not be largely affected. Most likely, the error is larger for Ag than for Pd, though, because Pd deposits onto the Ag template. If this is the case, then the %Ag values are a low estimate, meaning there could be more Ag in the nanostructure than reported. We believe that the calculations are close to the actual values, however, because the total moles of Pd plus Ag combined in the PdAg alloy was 88−128% of the original moles of Ag in the original pure Ag nanostructure after taking into account that each Pd displaces two Ag atoms. The range represents the standard deviation of the measurement, but this shows that we are oxidizing almost all of the metal during the LSV analysis, leading to only a small potential error.

■ CONCLUSIONS

The rate of the galvanic exchange process clearly has an effect on the final nanostructure morphology. The resulting morphology depends on the rate of the exchange reaction, which depends on the concentration of $PdCl_4^{2-}$. At low concentrations ($\leq 5.0 \times 10^{-5}$ M), the exchange occurred at the twin-plane defect sites along the NWs decorating them with small Pd or PdAg nanoparticles. Higher $PdCl_4^{2-}$ concentrations ($\geq 7.5 \times 10^{-5}$ M) led to a faster reaction rate, where Pd deposition and growth occurred on top of the Ag NWs more evenly over the entire surface. LSV allowed an estimation of the Ag and Pd composition on glass/ITO electrodes to correlate with the UV−vis and SEM data. The actual NW composition from electrochemical data did not match the composition determined by the normalized absorbance, likely because the optical properties are dominated by the surface composition, and the electrochemical data reflect the entire composition of the nanostructure. Electrochemical data also showed that the rate of exchange was slower than that expected for a diffusion-limited process and did not reach completion, leaving approximately 30% of Ag in the nanostructure after an hour of galvanic exchange for higher concentrations (0.5×10^{-4}−1.0×10^{-4} M) and approximately 75% for lower concentrations (0.10×10^{-4}−0.25×10^{-4} M). The slow rate and incompletion may be due to the greater stability of the PdAg alloy or inaccessibility to interior Ag atoms. The final morphology was a rough and likely hollow PdAg structure for the higher concentrations (30% Ag) at the completion of the reaction, but the detailed arrangement of Pd and Ag in the alloy is not known.

More experiments are still needed to understand the full details of galvanic exchange on 1D metals. This work represents an important step toward developing synthetic and surface

analytical methods to study the exchange process in order to reach that important goal.

■ ASSOCIATED CONTENT

Supporting Information. UV−vis spectra of exchange in all $PdCl_4^{2-}$ concentrations, plots of absorbance versus time with standard deviations, theoretical plots of %Ag as a function of time under diffusion-limited conditions, SEM images of hollow-looking structures, and %Ag and %Pd determined by linear sweep voltammetry as a function of exchange time. This material is available free of charge via the Internet at http://pubs.acs.org.

■ AUTHOR INFORMATION

Corresponding Author
*E-mail: f.zamborini@louisville.edu. Fax: 502-852-8149.

■ ACKNOWLEDGMENT

We thank Joe Williams for help with SEM imaging. We gratefully acknowledge the National Science Foundation (CHE-0848883) for full financial support of this research.

■ REFERENCES

(1) El-Sayed, M. A. *Acc. Chem. Res.* **2001**, *34*, 257.
(2) Ivanova, O. S.; Zamborini, F. P. *J. Am. Chem. Soc.* **2010**, *132*, 70.
(3) Ivanova, O. S.; Zamborini, F. P. *Anal. Chem.* **2010**, *82*, 5844.
(4) Burda, C.; Chen, X.; Narayanan, R.; El-Sayed, M. A. *Chem. Rev.* **2005**, *105*, 1025.
(5) Sardar, R.; Funston, A. M.; Mulvaney, P.; Murray, R. W. *Langmuir* **2009**, *25*, 13840.
(6) Law, M.; Sirbuly, D. J.; Johnson, J. C.; Goldberger, J.; Saykally, R. J.; Yang, P. *Science* **2004**, *305*, 1269.
(7) Liu, F.; Lee, J. Y.; Zhou, W. J. *Small* **2006**, *2*, 121.
(8) Narayanan, R.; El-Sayed, M. A. *J. Phys. Chem. B* **2005**, *109*, 12663.
(9) Feldheim, D. L.; Keating, C. D. *Chem. Soc. Rev.* **1998**, *27*, 1.
(10) Sudeep, P. K.; Joseph, S. T. S.; Thomas, K. G. *J. Am. Chem. Soc.* **2005**, *127*, 6516.
(11) Huang, X.; Neretina, S.; El-Sayed, M. A. *Adv. Mater.* **2009**, *21*, 4880.
(12) Bhattacharyya, S.; Saha, S. K.; Chakravorty, D. *Appl. Phys. Lett.* **2000**, *77*, 3770.
(13) Braun, E.; Eichen, Y.; Sivan, U.; Ben-Yoseph, G. *Nature* **1998**, *391*, 775.
(14) Caswell, K. K.; Bender, C. M.; Murphy, C. J. *Nano Lett.* **2003**, *3*, 667.
(15) Gao, Y.; Song, L.; Jiang, P.; Liu, L. F.; Yan, X. Q.; Zhou, Z. P.; Liu, D. F.; Wang, J. X.; Yuan, H. J.; Zhang, Z. X.; Zhao, X. W.; Dou, X. Y.; Zhou, W. Y.; Wang, G.; Xie, S. S.; Chen, H. Y.; Li, J. Q. *J. Cryst. Growth* **2005**, *276*, 606–612.
(16) Gou, L.; Chipara, M.; Zaleski, J. M. *Chem. Mater.* **2007**, *19*, 1755.
(17) Graff, A.; Wagner, D.; Ditlbacher, H.; Kreibig, U. *Eur. Phys. J. D* **2005**, *34*, 263.
(18) Han, Y.-J.; Kim, J. M.; Stucky, G. D. *Chem. Mater.* **2000**, *12*, 2068.
(19) Huang, M. H.; Choudrey, A.; Yang, P. *Chem. Commun.* **2000**, 1063.
(20) Jana, N. R.; Gearheart, L.; Murphy, C. J. *Chem. Commun.* **2001**, 617.
(21) Jiang, X.; Xie, Y.; Lu, J.; Zhu, L.; He, W.; Qian, Y. *J. Mater. Chem* **2001**, *11*, 1775.
(22) Liu, F.-K.; Huang, P.-W.; Chang, Y.-C.; Ko, C.-J.; Ko, F.-H.; Chu, T.-C. *J. Cryst. Growth* **2005**, *273*, 439.
(23) Murphy, C. J.; Sau, T. K.; Gole, A. M.; Orendoff, C. J.; Gao, J.; Gou, L.; Hunyadi, S. E.; Li, T. *J. Phys. Chem. B* **2005**, *109*, 13857.
(24) Ni, C.; Hassan, P. A.; Kaler, E. W. *Langmuir* **2005**, *21*, 3334.
(25) Sun, Y.; Gates, B.; Mayers, B.; Xia, Y. *Nano Lett.* **2002**, *2*, 165.
(26) Sun, Y.; Mayers, B.; Herricks, T.; Xia, Y. *Nano Lett.* **2003**, *3*, 955.
(27) Sun, Y.; Xia, Y. *Science* **2002**, *298*, 2176.
(28) Tsuji, M.; Matsumoto, K.; Miyamae, N.; Tsuji, T.; Zhang, X. *Cryst. Growth Des.* **2007**, *7*, 311.
(29) Ugarte, D.; Châtelain, A.; de Heer, W. A. *Science* **1996**, *274*, 1897.
(30) Wei, G.; Zhou, H.; Liu, Z.; Song, Y.; Wang, L.; Sun, L.; Li, Z. *J. Phys. Chem. B* **2005**, *109*, 8738.
(31) Wiley, B.; Sun, Y.; Mayers, B.; Xia, Y. *Chem.—Eur. J.* **2005**, *11*, 454.
(32) Zhou, Y.; Yu, S. H.; Wang, C. Y.; Li, X. G.; Zhu, Y. R.; Chen, Z. Y. *Adv. Mater.* **1999**, *11*, 850.
(33) Xiang, Y.; Wu, X.; Liu, D.; Li, Z.; Chu, W.; Feng, L.; Zhang, K.; Zhou, W.; Xie, S. *Langmuir* **2008**, *24*, 3465.
(34) Lee, Y. W.; Kim, M.; Kim, Y.; Kang, S. W.; Lee, J.-H.; Han, S. W. *J. Phys. Chem. C* **2010**, *114*, 7689.
(35) Cobley, C. M.; Xia, Y. *Mater. Sci. Eng. R* **2010**, *70*, 44.
(36) Moon, G. D.; Ko, S.; Min, Y.; Zeng, J.; Xia, Y.; Jeong, U. *Nano Today* **2011**, *6*, 186.
(37) Sun, Y.; Mayers, B.; Xia, Y. *Adv. Mater.* **2003**, *15*, 641.
(38) Sun, Y.; Xia, Y. *Nano Lett.* **2003**, *3*, 1569.
(39) Skrabalak, S. E.; Chen, J.; Au, L.; Lu, X.; Li, X.; Xia, Y. *Adv. Mater.* **2007**, *19*, 3177.
(40) Sun, Y.; Willey, B.; Li, Z.-Y.; Xia, Y. *J. Am. Chem. Soc.* **2004**, *126*, 9399.
(41) Sun, Y.; Xia, Y. *Adv. Mater.* **2004**, *16*, 264.
(42) Chen, J.; Willey, B.; McLellan, J.; Xiong, Y.; Li, Z.-Y.; Xia, Y. *Nano Lett.* **2005**, *5*, 2058.
(43) Chen, H. M.; Hsin, C. F.; Liu, R.-S.; Lee, J.-F.; Jang, L.-Y. *J. Phys. Chem. C* **2007**, *111*, 5909.
(44) Lu, X.; Au, L.; McLellan, J.; Li, Z.-Y.; Marquez, M.; Xia, Y. *Nano Lett.* **2007**, *7*, 1764.
(45) Sun, Y.; Tao, Z.; Chen, J.; Herricks, T.; Xia, Y. *J. Am. Chem. Soc.* **2004**, *126*, 5940.
(46) Camargo, P. H. C.; Xiong, Y.; Ji, L.; Zuo, J. M.; Xia, Y. *J. Am. Chem. Soc.* **2007**, *129*, 15452.
(47) Bansal, V.; Jani, H.; Plessis, J. D.; Coloe, P. J.; Bhargava, S. K. *Adv. Mater.* **2008**, *20*, 717.
(48) Bi, Y.; Lu, G. *Chem. Mater.* **2008**, *20*, 1224.
(49) Guo, S.; Dong, S.; Wang, E. *Chem.—Eur. J.* **2008**, *14*, 4689.
(50) Yoo, S.-H.; Park, S. *Adv. Mater.* **2007**, *19*, 1612.
(51) Teng, X.; Wang, Q.; Liu, P.; Han, W.; Frenkel, A. I.; Wen, W.; Marinkovic, N.; Hanson, J. C.; Rodriguez, J. A. *J. Am. Chem. Soc.* **2008**, *130*, 1093.
(52) Selvakannan, P.; Sastry, M. *Chem. Commun.* **2005**, 1684.
(53) Strasser, P.; Koh, S.; Greeley, J. *Phys. Chem. Chem. Phys.* **2008**, *10*, 3670.
(54) Liu, Y.-C.; Yang, S.-J. *Electrochim. Acta* **2007**, *52*, 1925.
(55) Cao, Z.; Xiao, D.; Kang, L.; Wang, Z.; Zhang, S.; Ma, Y.; Fu, H.; Yao, J. *Chem. Commun.* **2008**, 2692.
(56) Safaee, A.; Sarkar, D. K.; Farzaneh, M. *Appl. Surf. Sci.* **2008**, *254*, 2493.
(57) Tang, S.; Vongehr, S.; Zheng, Z.; Liu, H.; Meng, X. *J. Phys. Chem. C* **2010**, *114*, 18338.
(58) Lu, Y.; Chen, W. *J. Phys. Chem. C* **2010**, *114*, 21190.
(59) Wang, D.; Li, T.; Liu, Y.; Huang, J.; You, T. *Cryst. Growth Des.* **2009**, *9*, 4351.
(60) Huang, J.; Vongehr, S.; Tang, S.; Lu, H.; Meng, X. *J. Phys. Chem. C* **2010**, *114*, 15005.
(61) Slawinski, G. W.; Zamborini, F. P. *Langmuir* **2007**, *23*, 10357.
(62) Fang, J.; Ma, X.; cai, H.; Song, X.; Ding, B. *Nanotechnology* **2006**, *17*, 5841.
(63) Wang, C.-H.; Sun, D.-C.; Xia, X.-H. *Nanotechnology* **2006**, *17*, 651.

(64) Chen, Q.-S.; Sun, S.-G.; Zhou, Z.-Y.; Chen, Y.-X.; Deng, S.-B. *Phys. Chem. Chem. Phys.* **2008**, *10*, 3645.
(65) Sasaki, K.; Adzic, R. R. *J. Electrochem. Soc.* **2008**, *155*, B180.
(66) Yang, J.; Lee, J. Y.; Zhang, Q.; Zhou, W.; Liu, Z. *J. Electrochem. Soc.* **2008**, *155*, B766.
(67) Mahmoud, M. A.; Saira, F.; El-Sayed, M. A. *Nano Lett.* **2010**, *10*, 3764.
(68) Mohl, M.; Kumar, A.; Reddy, A. L. M.; Kukovecz, A.; Konya, Z.; Kiricsi, I.; Vajtai, R.; Ajayan, P. M. *J. Phys. Chem. C* **2010**, *114*, 389.
(69) Lu, X.; Tuan, H.-Y.; Chen, J.; Li, Z.-Y.; Korgel, B. A.; Xia, Y. *J. Am. Chem. Soc.* **2007**, *129*, 1733.
(70) Sun, Y.; Xia, Y. *J. Am. Chem. Soc.* **2004**, *126*, 3892.
(71) Skrabalak, S. E.; Chen, J.; Sun, Y.; Lu, X.; Au, L.; Cobley, C. M.; Xia, Y. *Acc. Chem. Res.* **2008**, *41*, 1587.
(72) Bi, Y.; Lu, G. *Chem. Commun.* **2008**, 6402.
(73) Lv, S.; Suo, H.; Wang, H.; Wang, C.; Wang, J.; Xu, Y.; Zhao, C. *Solid State Sci.* **2010**, *12*, 1287.
(74) Mieszawska, A. J.; Slawinski, G. W.; Zamborini, F. P. *J. Am. Chem. Soc.* **2006**, *128*, 5622.
(75) Block, B. P. *Inorg. Synth.* **1953**, *4*, 14.
(76) Gole, A.; Murphy, C. J. *Chem. Mater.* **2004**, *16*, 3633.
(77) Jana, N. R.; Gearheart, L.; Murphy, C. J. *J. Phys. Chem. B* **2001**, *105*, 4065.
(78) Matsumoto, T.; Kbayashi, K.; Fukami, K.; Sakka, T.; Ogata, Y. H. *Phys. Status Solidi C* **2009**, *6*, 1561.
(79) Chen, H.; gao, Y.; Zhang, H.; Liu, L.; Yu, H.; Tian, h.; Xie, S.; Li, J. *J. Phys. Chem. B* **2004**, *108*, 12038.
(80) Murray, B. J.; Li, Q.; Newberg, J. T.; Hemminger, J. C.; Penner, R. M. *Chem. Mater.* **2005**, *17*, 6611.